Oncogenic ZMYND11-MBTD1 fusion protein anchors the NuA4/TIP60 histone acetyltransferase complex to the coding region of active genes

Maeva Devoucoux, Gabriel Khelifi, Victoire Fort, Gaelle Bourriquen, Samer M. I. Hussein*, Jacques Côté*[#].

St. Patrick Research Group in Basic Oncology, Laval University Cancer Research Center, Oncology division of CHU de Québec-Université Laval Research Center, Quebec City, QC G1R 3S3, Canada.

*corresponding authors: samer.hussein@crchudequebec.ulaval.ca; jacques.cote@crchudequebec.ulaval.ca

[#]Lead contact

ABSTRACT

A chromosomal translocation found in cannibalistic acute myeloid leukemia (AML) leads to an in-frame fusion of the transcription elongation repressor ZMYND11 to MBTD1, a subunit of the NuA4/TIP60 histone acetyltransferase (HAT) complex. In contrast to the NuA4/TIP60 complex, ZMYND11 is linked to repression of actively transcribed genes through recognition of H3.3K36me3. To understand the abnormal molecular events that expression of this ZMYND11-MBTD1 fusion protein can create, we performed its biochemical and functional characterization in comparison to each individual fusion partner. ZMYND11-MBTD1 is stably incorporated into the endogenous NuA4/TIP60 complex but does not bring any additional interactors as the fusion lacks the MYND domain of ZMYND11. Nevertheless, this truncated ZMYND11 moiety in the fusion mostly leads to mislocalization of the NuA4/TIP60 complex on the body of genes normally bound by ZMYND11 in the genome. This can be correlated to increased chromatin acetylation and altered gene transcription, most notably on the *MYC* oncogene. Importantly, expression of ZMYND11-MBTD1, but not the individual fusion partners, during embryonic stem cell differentiation, leads to decreased expression of specific differentiation markers, while favoring Myc-driven pluripotency. Altogether, these results indicate that the ZMYND11-MBTD1 fusion protein functions primarily by mistargeting the NuA4/TIP60 complex to the body of genes, altering normal transcription of specific genes, likely driving oncogenesis in part through the Myc regulatory network.

Highlights:

-A recurrent chromosomal translocation detected in cannibalistic acute myeloid leukemia leads to the production of a ZMYND11-MBTD1 fusion protein.

-The ZMYND11-MBTD1 fusion protein is stably incorporated into the endogenous NuA4/TIP60 complex

-ZMYND11-MBTD1 leads to mistargeting of NuA4-TIP60 activity to the coding region of ZMYND11-target genes, altering gene expression and transcript isoforms.

-ZMYND11-MBTD1 binds the *MYC* gene leading to its upregulation, favoring growth and pluripotency while inhibiting differentiation markers.

KEYWORDS

ZMYND11, MBTD1, NuA4, TIP60, AML, translocation, protein fusion, MYC, chromatin, acetylation, transcription, mRNA processing.

INTRODUCTION

Acute myeloid leukemia (AML) is a type of hematological cancer characterized by an expansion of immature cells called blasts for undifferentiated myeloid precursors. This clonal expansion leads to impaired hematopoiesis and bone marrow failure. Although intensive chemotherapy induces a remission for many patients, relapse still occurs in some patients and the survival rate after relapse is poor (Döhner et al., 2015; Padella et al., 2019). So, understanding the molecular mechanism driving AML is necessary to improve treatment by identifying potential therapeutic targets that are more effective. It is already known that this cancer is due to the presence of genetic abnormalities such as somatic mutations and a significant number of gene fusions induced by chromosomal translocations (TCGA Research Network, 2013; Zjablovskaja and Florian, 2019). A specific recurrent translocation, t(10;17)(p15;q21), has been described over the past few years and has been linked to a cannibalistic form of AML (Plesa and Sujobert, 2019). Based on FISH analyses, this translocation creates a merge of *ZMYND11* and *MBTD1* genes (De Braekeleer et al., 2013). The break points are in exon 11 or 12 of *ZMYND11* and exon 3 of *MBTD1*, creating an in-frame coding sequence that encompasses a truncated ZMYND11 fused to a full-length MBTD1 (De Braekeleer et al., 2013; de Rooij et al., 2016; Plesa and Sujobert, 2019; Tempescul et al., 2007; Yamamoto et al., 2018) (**Fig. 1A**).

The nuclear factor ZMYND11 (also called BS69) contains a tandem reader module of the histone variant H3.3 trimethylation on lysine 36 (H3.3K36me3), including a PWWP domain, a plant homeodomain (PHD) and a bromodomain. It also contains a C-terminal MYND domain that is important for binding proteins such as transcription factors, the spliceosome machinery, and chromatin factors (Guo et al., 2014; Sugden et al., 2019; Velasco et al., 2006; Wang et al., 2014; Wen et al., 2014). Interestingly, these bindings confer

to ZMYND11 a function in pre-mRNA processing, mostly by promoting intron-retention (Guo et al., 2014). The *ZMYND11* gene is often deleted or downregulated in many types of cancer, including breast cancer (Chen et al., 2019). Moreover, overexpression of ZMYND11 inhibits tumor cell growth, highlighting a tumor suppressor function (Chen et al., 2019; Wen et al., 2014). Recently, it was shown that, in immune cells, stimulation-induced H3.3S31 phosphorylation leads to ejection of ZMYND11, allowing rapid transcriptional activation (Armache et al., 2020).

MBTD1 (Malignant Brain Tumor Domain-containing protein 1) was originally identified in the Polycomb Group family of proteins because of its 4 MBT domains. Knock-out of the *MBTD1* gene in mice leads to death soon after birth caused by defects in hematopoietic stem cells and skeletal formation (Hiroaki Honda et al., 2011). MBTD1 is a stable stoichiometric subunit of the large NuA4/TIP60 protein complex (Jacquet et al., 2016; Zhang et al., 2020). NuA4/TIP60 is highly conserved in eukaryotes, harboring histone acetyltransferase activity towards H4/H2A via the haploinsufficient tumor suppressor KAT5/Tip60 subunit as well as ATP-dependent histone exchange activity via the EP400 subunit (Pradhan et al., 2016; Steunou A-L et al., 2014). NuA4/TIP60 complex is an essential regulator of gene expression and genome stability, implicated in many cellular functions such as apoptosis and stem cell maintenance/renewal. The function of MBTD1 within NuA4/TIP60 has been linked to both gene-specific regulation and repair of DNA double-strand breaks through its MBT domains binding preference for the H4K20me1/2 histone mark (Jacquet et al., 2016; Jitka Eryilmaz et al., 2009; Zhang et al., 2020).

Well-characterized examples of fusions are found in AML, most notably translocations involving mixed-lineage leukemia 1 (MLL1) protein (KMT2A) which are found in up to 10% of acute leukemia (Winters and Bernt, 2017). These translocations have been

the focus of intense research to understand their oncogenic mechanism in order to improve therapy (Birch and Shilatifard, 2020; Zhao et al., 2019). The same interest and goals logically apply to the newly described *ZMYND11-MBTD1* translocation recurrently found in AML patients. Thus, we undertook biochemical and functional analyses of the fusion protein produced by this translocation. In this report, we describe the stable integration of the ZMYND11-MBTD1 fusion protein in the full NuA4/TIP60 complex. This leads to mislocalization of NuA4/TIP60 on the body of genes normally bound by ZMYND11. Associated changes in chromatin marks, gene expression and mRNA processing are analyzed, and events likely linked to the oncogenic mechanism of the ZMYND11-MBTD1 fusion are identified.

RESULTS AND DISCUSSION

The ZMYND11-MBTD1 fusion protein is stably incorporated into the endogenous NuA4/TIP60 acetyltransferase complex

In order to characterize the interactome of the ZMYND11-MBTD1 fusion protein, we used genome editing to integrate a single copy of tagged cDNAs at the *AAVS1* genomic safe harbor locus (Dalvai et al., 2015). We established isogenic K562 cell lines expressing 3xFlag-2xStrep-tagged ZMYD11-MBTD1, fusion partners truncated ZMYND11(aa1-409) and full-length MBTD1, as well as full-length ZMYND11 and empty tag as controls (**Fig. 1A-B**). Expression of the different constructs from isolated cellular clones is shown in **Fig. 1C**. Tandem affinity purifications were performed from nuclear extracts using anti-Flag and Strep-Tactin beads and native elution with Flag peptides and biotin, respectively (Doyon and

Côté, 2016). As we reported previously, through its stable association with EPC1, MBTD1 was purified along with all known subunits of NuA4/TIP60, as seen on silver-stained gel, western blot analysis and mass spectrometry (**Fig. 1B, D-E**, **Table S1**)(Jacquet et al., 2016; Zhang et al., 2020). ZMYND11 on the other hand was found mostly by itself but several associated substoichiometric proteins were detected, including previously linked EFTUD2 and other mRNA processing factors (**Fig. 1D-E**, **Table S1**)(Guo et al., 2014). In contrast, the truncated ZMYND11 found in the fusion lost almost all of these interactions, at least in part due to its missing MYND domain (**Fig. 1D-E**, **Table S1**)(Guo et al., 2014). Finally, purification of the ZMYND11-MBTD1 fusion protein produced an exact merge of the full NuA4-TIP60 complex with the simple addition of the truncated ZMYND11 moiety of the fusion (**Fig. 1D-E**, **Table S1**). These results indicate that the ZMYND11-MBTD1 fusion is stably incorporated in the endogenous NuA4/TIP60 complex, while not bringing any significant additional interactors. This suggests that the oncogenic mechanism of the fusion protein engages NuA4/TIP60 activities.

The ZMYND11-MBTD1 fusion protein hijacks the NuA4/TIP60 complex to the coding regions of genes

Since truncated ZMYND11 moiety of the fusion protein contains strong chromatin reader motifs (PHD-Bromo-PWWP) specific for the H3.3K36me3 mark (Guo et al., 2014; Wen et al., 2014), a logical hypothesis is that it will affect NuA4/TIP60 localization in the genome. While ZMYND11 follows H3.3K36me3 on the coding region of active genes (Guo et al., 2014; Wen et al., 2014), NuA4/TIP60 is normally localized around the transcription start sites and at a subset of enhancers (Jacquet et al., 2016; Ravens et al., 2015). Thus, to elucidate the genome-wide location of the ZMYND11-MBTD1 fusion protein, we performed chromatin

immunoprecipitations coupled to high throughput sequencing (ChIP-seq) using the tagged isogenic cell lines. As expected, MBTD1 and ZMYND11 bound regions showed strong enrichment for promoters and gene bodies, respectively (**Fig. 2A**). Interestingly, the truncated ZMYND11 lacking the MYND domain remained bound to almost all the same genome region as the full-length protein (**Fig. 2A-B**). This clearly indicates that ZMYND11 chromatin reader module (PHD-Bromo-PWWP) is the main if not sole determinant of ZMYND11 location in the genome. Finally, analysis of the ZMYND11-MBTD1 binding profiles showed enrichment at both promoters and gene bodies (**Fig. 2A**). But analysis of the total bound regions showed that almost all of them are shared with the truncated ZMYND11 locations (**Fig. 2B**). As expected, fusion-bound genomic locations are enriched for histone marks and transcription factors detected on active genes (**Table S2A**) while Gene ontology term (GO-term) enrichment analyses identify different biological processes, molecular functions, some pathways potentially involved in tumorigenesis (**Fig. S1A**). Interestingly, the ZMYND11-MBTD1 fusion tended to be enriched at the acceptor and donor splice sites on the coding region of genes, similar to WT ZMYND11 and truncated ZMYND11 but not MBTD1 (**Fig. S1B**). Altogether, these results indicate that the ZMYND11 moiety of the fusion drives its location in the genome, bringing along NuA4/TIP60. ChIP-seq binding profiles of ZMYND11-MBTD1 on specific genes clearly show correlation with wild type and truncated ZMYND11 on the body of these genes, supporting the concept of driving mislocalization of the NuA4/TIP60 complex along their coding region (**Fig. 2C, S1C**). Importantly, *RPSA* is naturally bound at its TSS by the NuA4/TIP60 complex, as shown here by the MBTD1 profile, while ZMYND11 and the fusion are found from the TSS to the body of the gene (**Fig. 2C**, top). Other genes of interest shown include *MYC*, *FASTK-TMUB1*, *HOXB2*, *RNASEH2C* and *GADD45A* (**Fig. 2C**, **S1C**). This binding to the coding regions of specific genes was confirmed

by ChIP-qPCR while also highlighting the very strong signals elicited by ZMYND11 and its truncated form, much less so for the fusion, most likely due to its lower expression (**Fig. 2D, 1C**)(signal at *RPSA* shown at the TSS). Since most if not all ZMYND11-MBTD1 fusion is incorporated in the NuA4/TIP60 complex (**Fig. 1C**), it is logical to predict that the fusion will have an impact on chromatin dynamics on the body of bound genes.

Aberrant H4ac and RNAPII enrichments on a subset of genes bound by the ZMYND11-MBTD1 fusion

To confirm that ZMYND11-MBTD1 leads to mislocalization of NuA4/TIP60 and its activity, we measured H4 acetylation by ChIP-qPCR on selected genes. While several genes did not show any significant changes of H4ac in cells expressing the fusion or its partners independently, we detected a clear increase of histone acetylation on the coding region of the *MYC* oncogene (and the *TMUB1* gene), specifically in the presence of the fusion (**Fig. 2E**). Since ZMYND11 binds to actively transcribed genes carrying the H3.3K36me3 mark, it is possible the fusion bringing NuA4/TIP60 activities has little visible impact on an already open highly dynamic chromatin, on which ZMYND11 may have little effect to start with. Nevertheless, we then focused on the clearly impacted *MYC* locus and analyzed H4ac at different locations along the gene (**Fig. 2F**). The increase of acetylation specific to the fusion-expressing cells is localized over the central exon of the MYC gene, exactly where ZMYND11 and the fusion are enriched on their ChIP-seq profiles (**Fig. 2F vs 2C**). These results clearly demonstrate that the ZMYND11-MBTD1 fusion does bring the NuA4/TIP60 complex and mis-targets its acetyltransferase activity on the coding region of the *MYC* oncogene.

Normally, histone acetylation is enriched over the promoter/TSS region where the H3K4me3 mark is located but decreases along the coding region with the appearance of the

H3K36me3 mark as chromatin needs more stability to avoid spurious transcription (Barth and Imhof, 2010). We then asked if the change of H4 acetylation induced by the ZMYND11-MBTD1 fusion has an impact on these methylation marks. We could not see any fusion-specific changes on *MYC* or *RPSA*, only maybe some effect of the fusion partners by themselves (**Fig. S1D-E**). Next, we looked at the density of RNA polymerase II (RNAPII) as local changes in chromatin dynamics due to increased acetylation may affect elongation. Total RNAPII measured by ChIP-qPCR along the *RPSA* gene showed a strong increase of signal specifically at the TSS in cells expressing the fusion (**Fig. 2G**). Interestingly, this was also seen in cells expressing the truncated ZMYND11 but not the wild type form. truncated ZMYND11 and the fusion expression compared to control cell lines (**Fig. 2G**). Thus, these effects seem independent of NuA4/TIP60 and its HAT activity (**Fig. 2E**) and are likely produced somehow by the loss of the MYND domain in ZMYND11. In contrast, RNAPII signals were clearly increased by the ZMYND11-MBTD1 fusion at 3 locations along the *MYC* gene (**Fig. 2H**). These results suggest that mis-targeting of NuA4/TIP60 activity by the ZMYND11-MBTD1 fusion can lead to increased transcription on genes like the *MYC* oncogene and this could be part of the oncogenic mechanism.

The ZMYND11-MBTD1 fusion protein alters the expression of several genes linked to growth and differentiation

To get a bigger picture of the effect of ZMYND11-MBTD1 on gene expression, we use CRISPR/Cas9 to knock-out the endogenous *ZMYND11* gene (Agudelo et al., 2017) in our K562 cell lines expressing the fusion protein or its partners from the *AAVS1* locus. We used two gRNAs to induce a truncation in the C-terminal MYND domain of endogenous ZMYND11 and isolated 2 independent clones (**Fig. S2A-C**). We kept the MBTD1-AAVS1 cell line that still

expressed endogenous ZMYND11 as a control. Taking advantage of the Oxford Nanopore Technologies long-read Sequencing, a nanopore-based single-molecule sequencing that is more informative for gene isoform/splice variant characterization (Jason L Weirather et al., 2017), we sought to determine changes in mRNA levels upon expression of the ZMYND11-MBTD1 fusion compared to its fusion partners. Differential mRNA expression was investigated comparing sequences between the fusion cell lines (endogenous ZMYND11 KO + ZMYND11-MBTD1) and three control cell line pairs (endogenous ZMYND11-wild type + MBTD1-AAVS1 (control), ZMYND11-KO + MBTD1-AAVS1 (MBTD1) and ZMYND11-KO + truncated ZMYND11-AAVS1 (tr.ZMYND11)). 340 genes were found upregulated and 446 downregulated in the cells expressing the ZMYND11-MBTD1 fusion expression compared to both partners in the fusion individually (**Fig. 3A**). Interestingly, gene ontology analyses show that the genes upregulated are enriched for ribosome biogenesis, hence supporting growth/proliferation, and downregulated genes are strongly enriched for biological processes involved in myeloid cell activation, which likely reflects K562 cells undergoing some dedifferentiation programming, a hallmark of oncogenesis (**Fig. 3B**). Importantly, more than 50% of these dysregulated genes are directly bound by the ZMYND11-MBTD1 fusion protein based on our ChIP-seq data (**Table S2B**). Thereafter, we used RT-qPCR to validate 2 genes upregulated and important positive regulators of cell growth/proliferation, *MYC* and *AKT2*, and confirmed their increased expression in cells expressing the ZMYND11-MBTD1 fusion compared to the control cell lines (**Fig. 3C**). Interestingly, a significant portion of the genes affected by the fusion are known to be regulated by MYC/MAX transcription factors, suggesting indirect effect on their transcription due to increased expression of MYC (**Table S2C**). These results argue that the specific expression of the ZMYND11-MBTD1 fusion

protein and its association to NuA4/TIP60 lead to transcription changes of several ZMYND11-target genes, favoring cell growth/proliferation and inhibiting differentiated phenotypes.

The ZMYND11-MBTD1 fusion protein disrupts gene-specific ratio of mRNA splice variants

Almost 95% of human mRNAs are alternatively spliced and many studies already proved that chromatin marks affect splicing (for review (Hnilicova and Stanek, 2011)). Moreover, ZMYND11 itself was shown to interact with splicing factors and directly affect splicing events, especially intron retention (Guo et al., 2014). However, we have shown here that ZMYND11 normal interactome is lost in the fusion and that local chromatin structure can be affected by mislocalization of NuA4/TIP60 on ZMYND11-target gene bodies (**Fig. 1, 2**). It was then important to determine whether the fusion protein perturbs normal mRNA splicing events causing different gene isoforms to be expressed. We first correlated changes in gene expression compared to their corresponding transcripts levels in K562 cells wild type (ZMYND11-WT + MBTD1-AAVS1) and KO for endogenous ZMYND11 (ZMYND11-KO + MBTD1-AAVS1) (**Fig. 3D**, left panel). Several transcripts showed differential expression compared to the overall corresponding gene expression (highlighted in blue color) suggesting that the knock-out of ZMYND11 affects mRNA splicing. We then compared differential isoform expression in ZMYND11-KO + ZMYND11-MBTD1 (fusion) to its control partners ZMYND11-KO + MBTD1-AAVS1 (MBTD1) (**Fig. 3D**, middle panel) and ZMYND11-KO + truncated ZMYND11-AAVS1 (tr.ZMYND11) (**Fig. 3D**, right panel). Differential isoform expression found per single comparison are highlighted in blue color. Transcripts that changed significantly in both fusion comparisons (**Fig. 3D**, middle and right panels) but not in the control comparison (**Fig. 3D**, left panel) are highlighted in orange color. We identified 150 transcripts that are significantly deregulated by the fusion protein. Importantly, almost

80% of the corresponding genes are bound by the ZMYND11-MBTD1 fusion and 65% are already known to be alternatively spliced. This was further confirmed by RT-qPCR of two selected genes in which the cells expressing the fusion protein specifically changed the ratio of splice variants compared to its partners and control cell lines (**Fig. 3E-F**). Altogether, these data demonstrate prominent specific effects of the ZMYND11-MBTD1 fusion on gene expression and transcript isoforms levels, part of the mechanism that is likely at play in acute myeloid leukemia harboring this chromosomal translocation.

The ZMYND11-MBTD1 fusion protein favors growth and inhibits expression of differentiation markers

ZMYND11 and KAT5/Tip60 are already known to have a tumor suppressor function and to be downregulated in many human cancers (Gorrini et al., 2007; Wen et al., 2014). We first compared growth inhibitory function by clonogenic assay in U2OS cells. As expected, overexpression of MBTD1 and ZMYND11 decreased the ability of U2OS cells to form colonies (**Fig. 4A, S2D**). In contrast, similar level of overexpression of the ZMYND11-MBTD1 fusion did not decrease colony formation compared to control. We then expressed the fusion, its partners and empty vector in mouse embryonic stem cells (mESCs) (**Fig. S2E**) undergoing spontaneous differentiation. RT-qPCR was used to monitor the expression of different sets of genes linked to pluripotency, embryonic germ layers and other early differentiation markers. Expression of early differentiation markers, such as *Brachyury* (mesoderm), *Sox17* (endoderm), and *Pax3* (neural epithelium and early neural crest) were downregulated by the over-expression of ZMYND11-MBTD1 fusion, although only *Pax3* and *Brachyury* were specific to the fusion expressing cells compared to control cells (**Fig. 4B, S2F-G**). Nonetheless, these results demonstrate that expression of the fusion protein inhibits differentiation of ESCs,

which is consistent with its oncogenic properties. In line with this notion, *Stella* (*Dppa3*/*Pgc7*) and *Myc*, which are markers of pluripotency, were upregulated specifically in cells expressing the fusion (**Fig. 4B**). Importantly, Stella, a H3K9me reader and inhibitor of DNA demethylation, has been implicated in a Myc-driven self-reinforcing regulatory network that maintains mESC identity, independently of Sox2 and Oct4 (Fagnocchi et al., 2016). These additional data further support ZMYND11-MBTD1 being a driver of oncogenic transformation, negating the natural tumor suppressor functions of ZMYND11 and NuA4/TIP60.

Conclusions

The recurrent chromosomal translocation t(10;17) (p15;q21) found in cannibalistic acute myeloid leukemia leads to the production of a fusion protein linking two factors with tumor suppressor activity, ZMYND11 and MBTD1. This physical merge disrupts ZMYND11 interactome with the mRNA processing machinery but not its strong epigenetic reader affinity for H3.3K36me3 located on the coding region of transcribed genes. As the fusion protein is stably integrated into the NuA4/TIP60 complex, it leads to mislocalization of this important chromatin modifier/remodeler complex to the body of genes, altering chromatin dynamics, transcription elongation and co-transcriptional mRNA processing events on specific genes (see model in **Fig. 4C**). In contrast to its fusion partners, ZMYND11-MBTD1 favors cell growth/proliferation, likely in part through expression of the *MYC* oncogene, and inhibits expression of specific differentiation markers. As mistargeting of the NuA4/TIP60 complex seems to be the main mechanism employed by the fusion, it will be most interesting to test some specific KAT5/Tip60 HAT inhibitors (Gao et al., 2014) (Coffey et al., 2012) to determine if de novo acetylation at coding regions is indeed the main oncogenic

driving force in this specific group of acute myeloid leukemia. For potential therapeutic approaches, inhibiting the HAT activity of KAT5/Tip60 may have large pleiotropic effects due to the essential roles of NuA4/TIP60 in many nuclear processes. Since we recently described the structural determinants by which MBTD1 associates with NuA4/TIP60 through the EPC1 subunit (Zhang et al., 2020), an alternative more specific approach would be to design small molecules that disrupt this interaction and, in the present case, detach the ZMYND11-MBTD1 fusion protein from the NuA4/TIP60 complex in these leukemic cells.

EXPERIMENTAL PROCEDURES

Establishment of isogenic cell lines using the *AAVS1* safe harbor.

K562 cells were used to isolate clones after genome editing to stably express from the *AAVS1* safe harbor various 3xFlag2xSrep-tagged proteins from the moderately active human *PGK1* promoter, including MBTD1, ZMYND11, truncated ZMYND11 [aa1-409], and the ZMYND11-MBTD1 fusion, as described previously (Dalvai et al., 2015).

Affinity purification of complexes

Native complexes were purified essentially as described before (Dalvai et al., 2015). Briefly, Nuclear extracts were prepared from $2.5.10^9$ cells and pre-cleared with CL6B sepharose beads. FLAG immunoprecipitations with anti-Flag agarose affinity resin (Sigma M2) were performed followed by two elutions with 3xFLAG peptide in elution buffer (20 mM HEPES-KOH [pH 7.9], 10% glycerol, 150 mM KCl, 0.1% Tween 20, 1mMDTT, 1 mM PMSF, 2 mg/mL Leupeptin, 5 mg Aprotinin, 2 mg/mL Pepstatin, 10 mM Na-butyrate, 10 mM b-glycerophosphate) with 200 ug/mL 3xFLAG peptide (Sigma). Then, STREP immunoprecipitations with Strep-tactin sepharose beads (Cedarlane) were performed followed by two elutions with elution buffer supplemented by 4mM biotin. Typically, 20µL of the first elution Strep was loaded on Nu-PAGE 4%–12% Bis-Tris gels (Invitrogen) and analyzed via silver staining.

Mass spectrometry analysis

Affinity purified materials were resolved on a short SDS-PAGE gel, in-gel digested with trypsin, and subsequently analyzed by LC-MS/MS using an Agilent 1100 HPLC system (Agilent Technologies) coupled to a TripleTOFTM 5600 instrument at the proteomics platform of CHU de Québec-Université Laval Research Center. The data generated by the mass spectrometers were analyzed using Scaffold 4.

Antibodies

The following antibodies were used for Western blotting at the indicated dilution: anti-FLAG -HRP conjugate (Sigma M2 A8592-1MG, 1:5000); anti-MBTD1 (Abcam ab116361, 1:1000); anti-Brd8 (Bethyl A300-219A, 1:10000); anti-P400 (Abcam ab5201, 1:1000); anti-TRRAP (bethyl A301-132A, 1:2000); anti-MRG15 (Active Motif 39361, 1:1000); anti-Tip60 (Ab 137518, 1:1000); anti-GAPDH (ThermoFisher, 39-8600- ZG003, 1/25000).

ChIP-seq experiments

For Flag ChIP, 1mg of cross-linked chromatin from K562 cells was incubated with 10µg of anti-Flag antibody (Sigma, M2) pre-bound on 300 µl of Dynabeads Prot-G (Invitrogen) overnight at 4°C. The beads were washed extensively and eluted in 0.1% SDS, 0.1M NaHCO3. Crosslink was reversed with 0.2M NaCl and incubation overnight at 65C. Samples were treated with RNase and Proteinase K for 2h and recovered by phenol-chloroform and ethanol precipitation. Libraries for sequencing were prepared with TruSeq LT adaptors (Illumina). Samples were sequenced by 50 bp single reads on HiSeq 4000 platform (Illumina).

Processing, alignment and peak calling of ChIP-seq data

FastQ format reads were aligned to the hg19 human reference using the Bowtie alignment algorithm (Langmead et al., 2009). Bowtie2 version 2.1.6 was used with the pre-set sensitive parameter to align ChIP sequencing reads. MACS version 2.0.10 (model-based analysis of ChIPseq) peak finding algorithm was used to identify regions of ChIP-Seq enrichment over the background (Feng et al., 2012). The pipeline, commands, and parameters that were used are : Trimming of sequence (filter out 39 adaptor, and remove last 2 bases and 3 extra bases if it matches with adaptor sequence). Mapping sequences to human genome (hg19) using Bowtie: (i) command: bowtie2 -p 8 –sensitive -x genome/genome -U sequence.reads.fastq –S sample.sam. Peak calling algorithm MACS: (i) command : macs2 callpeak -t

ChIPseq.data.bam -c input.sample.file.bam --broad -f BAM -g hs -n [directory] –outdir MACS2_files --nomodel --shiftsize 100 –B. Unique mapped read values were normalized to library size. Peaks were annotated as per human genome EnsDb.Hsapiens.v75 – hg19.

ChIP-qPCR

ChIP was performed according to the protocol described in (Avvakumov et al., 2011). Briefly, 1mg of chromatin for Flag-ChIP (Flag-M2-Sigma) or anti-IgG antibody (Millipore- PP64). Also, 200 µg of chromatin were immunoprecipitated using 1-3µg of the following antibodies: anti-H4penta-Acetyl (Upstate 06-946), anti-H3 (Abcam ab1791), anti-H3K4me3 (Abcam Ab8580), anti-H3K36me3 (Abcam Ab9050), anti-RNAPII (8WG16 Covance), anti-phosphoSer2-CTD-RNAPII (Abcam 5095) overnight at 4C and incubated with 50ul of Dynabeads Protein A/G (Invitrogen) 4h at 4C. The beads were washed extensively and eluted in 0.1% SDS, 0.1M NaHCO3. Crosslink was reversed with 0.2M NaCl and incubation overnight at 65C. Samples were treated with RNase and Proteinase K for 2h and recovered by phenol-chloroform and ethanol precipitation. Quantitative real-time PCRs were performed on a LightCycler 480 (Roche) with SYBR Green I (Roche) to confirm the specific enrichment at defined loci compared to intergenic regions or negative locus. IgG-ChIPs were subtracted from FLAG-ChIP.

Primers	Sequences
intergchr12 for	AAGGGGCCTGAGTTCTTCTC
intergchr12 rev	CACAGCTTCCATCTGGCTCT
RPSA for	AGAAAGCGGGCTAACATCCT
RPSA rev	GCTGTGCTGTCACCACTTGT
RPSA 1 for	TGGCACTAGAAACCCCAAAG
RPSA 1 rev	GCAGGTAGCACGGAAAAGAC

RPSA 2 for	ATTTTCACAATGTCCGGAGCC
RPSA 2 rev	CTGGAAGTCAAGATTGGTGCC
RPSA 3 for	ACGGCTTCTTGTGGTTACTGA
RPSA 3 rev	CCACATAGCGCAGAGGAGAAT
FASTK for	TAACTTAACCCCTTCGCTGCT
FASTK rev	TCTCTGATGCTCCTTACACGC
TMUB1 for	CGTCTTAGTGTTCTGCCGGA
TMUB1 rev	AGTTACTTTAATCTGCACGGGT
RNASEH2C for	GAGAAGAAGGTGTCGATGGGG
RNASEH2C rev	AACCCTATCCCTTTGCTCACG
GADD45A for	GTGGTGCTTGCATTCGAGAG
GADD45A rev	ACCTTATCCATCCTACACGCG
HoxB2 for	TAATAAGTACCTGTGCCGGCC
HoxB2 rev	CTTCATGCGCCGGTTCTGAAA
MYC 1 for	ATGCCCCTCAACGTTAGCTT
MYC 1 rev	TGCTGCTGGTAGAAGTTCTCC
MYC 2 for	CCACCTCCAGCTTGTACCTG
MYC 2 rev	GAGAAGGCGCTGGAGTCTTG
MYC 3 for	GAACACACAACGTCTTGGAGC
MYC 3 rev	GGGGCCTTTTCATTGTTTTCCA
MYOD for	CGCCTGAGCAAAGTAAATGAG
MYOD rev	GATATAGCGGATGGCGTTG

CRISPR/Cas9-mediated KO of ZMYND11 in K562 cells

K562 CRISPR KO cell lines were established as described in (Agudelo et al., 2017) using two gRNAs to remove a full exon in C-term of ZMYND11 in AAVS1 cell lines expressing MBTD1 WT or truncated ZMYND11 or the ZMYND11-MBTD1 fusion. MBTD1 WT AAVS1 cell line is used as control. Target sequence for ZMYND11 (5'-ACACGCCGTCGTTTGTGGTCTGG-3') was built in eSpCas9 pX330 backbone and (5’- ATTAACGGGCATCATACCTGTGG-3’) was built in MLM3636 backbone. For targeting with the CRISPR/Cas9 system, 4.10^5 cells were transfected with 3 µg of each gRNA plasmid by Lipofectamine 3000 (Thermo Fisher). Three days post-transfection, cells were selected with ouabain. 5 days post-selection, cells were diluted for colony isolation and amplification followed by PCR screening. KO clones were validated by PCR screening, sequencing of the alleles, and RT-qPCR. *36B4* locus is used as control.

RNA extraction was performed with Monarch Total RNA Miniprep Kit (NEB #T2010) following the manufacturer’s indications. Then, 1µg of RNA was reverse transcribed by oligo-dT and random priming into cDNA with a qScript cDNA SuperMix kit (QuantaBio-VWR), according to the manufacturer’s instructions. Quantification of the amount of cDNA was done with SYBR Green I (Roche) on a LightCycler 480 (Roche). For real-time PCR, RNA samples from 2 different validated KO clones were compared to 2 WT control. The following primers are used to validate KO ZMYND11 clones by PCR and RT-qPCR: PCR for (5’-ATTATGTGGCTTCGTTTGGC-3’); PCR rev (5’-TGAGCAGTACACAGTAATATGGG-3’); RT-qPCR RPLPO for (5’- CGACCTGGAAGTCCAACTAC-3’); RPLPO rev (5’-ATCTGCTGCATCTGCTTG-3’); ZMYND11 N-term for (5’- ATGTCTCGAGTCCACGGTATG-3’); ZMYND11Nterm rev (5’-GCCCATCTCCTGTTTGTTTGT-3’); ZMYND11 C-term for (5’-CCAAGAATGCTGCATCGGAG-3’); ZMYND11 C-term rev (5’-CTTCCATTTCAGAACGCAGCT-3’).

Library preparation and long-read RNA-sequencing

Cell lysates were homogenized with QIAshredder columns (QIAGEN #79654) and total RNA was extracted with RNeasy mini columns (QIAGEN #74104). RNA was DNase treated using TURBO DNase (ThermoFisher Scientific #AM2238). RNA quality was verified on a 2100 Bioanalyzer (Agilent Technologies) and polyadenylated RNA was enriched using NEBNext Poly(A) mRNA Magnetic Isolation Module (NEB # E7490L). Libraries were generated using 100 ng of poly(A)+ RNA and Oxford Nanopore Technologies' Direct cDNA Sequencing Kit (ONT SQK-DCS109), with each sample barcoded with the Native Barcoding Expansion (ONT EXP-NBD104), according to the manufacturer's specifications. Barcoded samples were pooled, loaded on a MinION sequencer using four R9 Flow Cells (ONT FLO-MIN106D), and sequenced using the MinKNOW software v19.

Long-read RNA-seq data analysis

Raw fast5 files were basecalled using Guppy v.4.2.2 with the guppy_basecaller command and the dna_r9.4.1_450bps_fast.cfg configuration file and default settings. Barcodes were detected and reads were separated with the guppy_barcoder using the default settings. The resulting FASTQ reads were aligned to the hg19 human reference with Minimap2 with the following parameters: -aLx splice --cs=long. Raw read counts were obtained with the featureCounts tool from the Subread package v 2.0.0, using the exon counting mode (Li, 2018; Liao et al., 2014).

EdgeR R-package (v3.12.1) was then used to normalize the data, calculated RNA abundance at the gene and transcript levels (as counts per million reads (CPM), and perform statistical analysis (Robinson et al., 2010). Briefly, a common biological coefficient of variation (BCV) and dispersion (variance) were estimated based on a negative binomial distribution model. This estimated dispersion value was incorporated into the final EdgeR analysis for

differential gene expression, and the generalized linear model (GLM) likelihood ratio test was used for statistics, as described in EdgeR user guide.

Differential splicing analysis

Analysis of variations in splice isoform expression was performed by comparing differential expression at the gene and transcript levels. From all genes showing no differential expression with the selected control (FDR ≥ 0.1), those with significant differences in transcript expression (p-value ≤ 0.05, FDR ≤ 0.1) were selected. To highlight the genes with high changes in transcript expression compared to gene expression, a cutoff of 2-fold difference was applied to the Log2(fold change) values between the selected sample and control.

Reverse Transcription-qPCR

In ZMYND11 KO K562 cells stably expressing ZMYND11-MBTD1 fusion, MBTD1, WT ZMYND11, truncated ZMYND11 or empty vector, total RNA was extracted with Monarch Total RNA Miniprep Kit. 1ug of RNA was reverse transcribed by oligo-dT and random priming into cDNA with a qScript cDNA SuperMix kit (QuantaBio-VWR), according to the manufacturer's instructions.

Primers	Sequences
RPLP0 for	CGACCTGGAAGTCCAACTAC
RPLP0 rev	ATCTGCTGCATCTGCTTG
MYC for	GTCCTCGGATTCTCTGCTCTC
MYC rev	CTTCCTCATCTTCTTGTTCCTCC
AKT2 for	CCGCTACTACGCCATGAAGAT

AKT2 rev	AACGGGTGCCTGGTGTTC
NAT14 for	CTTGTCGAAGGACCAAAGG
NAT14 rev	TCATCTCCCGCACTGAC
NAT14-204 for	CCCAACTCTTCAAAGCACAG
NAT14-204 rev	GAAGTAAGGACAGGGAGGTT
SCAMP4 for	CCAGCCATCATGTTCTCCGT
SCAMP4 rev	CACTCCGTCTGTGCCTTCTG
SCAMP4-204 for	GCGTCGAAGTTTGTGTCCAC
SCAMP4-204 rev	AAGCGATACTGAGAGGCACC

Clonogenic growth assay

MBTD1, ZMYND11 ^{wt}, truncated ZMYND11 [1-409], the ZMYND11-MBTD1 fusion or empty vectors were transfected into U2OS cells which were then seeded onto dishes in duplicates. Subsequently, puromycin [1µg/µl] was added to the culture media at 48hours post-transfection for selection. After ten days of culture, the colonies formed on the dishes were fixed with methanol, followed by staining with crystal violet (Sigma C6158) and washing with distilled water. Images of the dishes were then taken.

Overexpression of ZMYND11 and MBTD1 constructs during mouse ESC differentiation

R1 mouse embryonic stem cells (ESCs) were culture in 2i-LIF medium (LIF: Leukemia Inhibitory Factor at 20 ng/mL, 3µ CHIR99021 (Cedarlane Labs #S2924), and 1µM PD0325901 (Cedarlane Labs #S1036) in N2B27 media). N2B27 media consists of a 1:1 mixture of DMEM/F-12 media mix (ThermoFisher Scientific # 11330057) supplemented with N2 supplement (ThermoFisher Scientific #17502048) and neurobasal media (ThermoFisher Scientific #21103049) supplemented with 1X B27 supplement (Thermo Fisher Scientific

#17504044), 1 mM sodium pyruvate, 2 mM L-glutamine, and ß-mercaptoethanol (10^{-4} M). For transfections, R1 ESCs were seeded on 0.1% gelatin in 2i-LIF medium at 125,000 cells/well in 6-well plates. The following day, the cells were transfected with the indicated constructs using Lipofectamine™ Stem Transfection Reagent (ThermoFisher Scientific #STEM00001) following the manufacturer's instructions, with 2 µg of DNA and 5 µL of lipofectamine/well. Cells were selected for 2 days with puromycin (1 µg/mL) in FBS-LIF medium (15% FBS plus LIF at 20 ng/mL, 1 mM sodium pyruvate, 2 mM L-glutamine, and ß-mercaptoethanol (10^{-4} M) in DMEM high-glucose) and then seeded on 0.1% gelatin in N2B27 medium (140,000 cells/dish in 6cm-dishes). Medium was changed 2 days later and cells were harvested 4 days post seeding in N2B27 medium. Total RNA was extracted using the EZ-10 Total RNA Miniprep Kit (BioBasic #BS88583) and DNase I (RNAse-free, 1U/µL)-treated (ThermoFisher Scientific #EN0521) following the manufacturers' instructions. RNA was reverse-transcribed for RT-qPCR using iScript™ gDNA Clear cDNA Synthesis Kit (BioRad #1725035) following the manufacturer's instructions. The mean relative fold-change in mRNA expression was normalized to *Rps13* housekeeping gene expression in the control condition (empty vector). The error bars represent the Standard Deviation (STD). Refer to table below for primer sequences.

Target gene	Primer	Primer sequence (5'->3')
Brachyury	Forward Reverse	ACCAACAAGCTCAATGGAGGG TCACGATGTGAATCCGAGGT
c-Myc	Forward Reverse	GAGGAGCTGGAATCTCTCGTG GCTGAAGCTTACAGTCCCAAAG
Cer1	Forward Reverse	AGCCAAGAGGTTCTGGCATC CCCAGTGTACTTCGTGGCTT
Esrrb	Forward Reverse	TGGTGCGCAGGTACAAGAAA CGCCTCCAGGTTCTCAATGT
l-Myc	Forward Reverse	GAGCGAGGGAGCGGACAT CGTGGAGCGGTAGAAATCCT
Mixl1	Forward	ACGCTCCCTCAGTAACAACG

	Reverse	AAGCTGCCACAGACTTCCAA
Nanog	Forward	ATGCCTGCAGTTTTTCATCC
	Reverse	GAGGCAGGTCTTCAGAGGAA
Oct 4	Forward	ACTGCTCTGGGCTCTCCCATGC
	Reverse	TACCTCCCTTGCCTTGGCTCACAG
Pax3	Forward	CATACCAGCTGTCGGAGACC
	Reverse	GACGGTGCTACTGGGATCTG
Pax6	Forward	CACCCGGCAGAAGATCGTAG
	Reverse	GTCTGATGGAGCCAGTCTCG
Pitx2	Forward	CATCCCCAGGCGTTAGCCAT
	Reverse	GGCCCTTATCTTTCTCTGCGAC
Rps13	Forward	TGATTTCCTGTGCCGTTTCCT
	Reverse	CGTGCATGCGACCCATGAT
Sox1	Forward	GCTGCTTAGCCTACCGCTTA
	Reverse	CCTGAGGCTATTGGGGCATT
Sox2	Forward	GAACGGCTGGAGCAACGGCA
	Reverse	CAGGGCGCTGACGTCGTAGC
Sox17	Forward	CCCAACACTCCTCCCAAAGTA
	Reverse	GAAAACAGTAGCGGGTCCAGA
Stella	Forward	AGAGAAGGGTCCGCACTTTG
	Reverse	AATGGCTCACTGTCCCGTTC

DATA availability

Sequencing data for both ChIP-seq and long read RNA-seq datasets are in the process of deposition at the GEO public database.

Acknowledgements

We thank members of the Côté laboratory for helpful discussion during the course of this project, and the Proteomics Center at CHU de Quebec Research Center for protein identification by mass spectrometry. This work was supported by grants from the Canadian Institutes of Health Research (CIHR) to J.C (FDN-143314) and S.M.I.H (PJT-378019). V. Fort is a recipient of a training award of the Fonds de Recherche du Québec-Santé (FRQ-S). G. Khelifi is a recipient of a Pierre J. Durand scholarship from the faculty of Medicine of Laval University and Luc Bélanger prestige scholarship of the CHU de Québec foundation. S.M.I.H

is a Junior 1 Research Scholar of the Fonds de Recherche du Québec-Santé. J.C. holds the Canada Research Chair in Chromatin Biology and Molecular Epigenetics.

REFERENCES

Agudelo, D., Duringer, A., Bozoyan, L., Huard, C.C., Carter, S., Loehr, J., Synodinou, D., Drouin, M., Salsman, J., Dellaire, G.*, et al.* (2017). Marker-free coselection for CRISPR-driven genome editing in human cells. Nature Methods *14*, 615-620.

Armache, A., Yang, S., Martinez de Paz, A., Robbins, L.E., Durmaz, C., Cheong, J.Q., Ravishankar, A., Daman, A.W., Ahimovic, D.J., Klevorn, T.*, et al.* (2020). Histone H3.3 phosphorylation amplifies stimulation-induced transcription. Nature *583*, 852-857.

Avvakumov, N., Lalonde, M.E., Saksouk, N., Paquet, E., Glass, K.C., Landry, A.J., Doyon, Y., Cayrou, C., Robitaille, G.A., Richard, D.E.*, et al.* (2011). Conserved Molecular Interactions within the HBO1 Acetyltransferase Complexes Regulate Cell Proliferation. Molecular and Cellular Biology *32*, 689-703.

Barth, T.K., and Imhof, A. (2010). Fast signals and slow marks: the dynamics of histone modifications. Trends Biochem Sci *35*, 618-626.

Birch, N.W., and Shilatifard, A. (2020). The role of histone modifications in leukemogenesis. Journal of biosciences *45*.

Chen, Y.U.N., Tsai, Y.-H., and Tseng, S.-H. (2019). Regulation of BS69 Expression in Cancers. Anticancer Research *39*, 3347-3351.

Coffey, K., Blackburn, T.J., Cook, S., Golding, B.T., Griffin, R.J., Hardcastle, I.R., Hewitt, L., Huberman, K., McNeill, H.V., Newell, D.R.*, et al.* (2012). Characterisation of a Tip60 specific inhibitor, NU9056, in prostate cancer. PLoS One *7*, e45539.

Dalvai, M., Loehr, J., Jacquet, K., Huard, Caroline C., Roques, C., Herst, P., Côté, J., and Doyon, Y. (2015). A Scalable Genome-Editing-Based Approach for Mapping Multiprotein Complexes in Human Cells. Cell Reports *13*, 621-633.

De Braekeleer, E., Auffret, R., Douet-Guilbert, N., Basinko, A., Le Bris, M.-J., Morel, F., and De Braekeleer, M. (2013). Recurrent translocation (10;17)(p15;q21) in acute poorly differentiated myeloid leukemia likely results in ZMYND11–MBTD1 fusion. Leukemia & Lymphoma *55*, 1189-1190.

de Rooij, J.D.E., van den Heuvel-Eibrink, M.M., Kollen, W.J.W., Sonneveld, E., Kaspers, G.J.L., Beverloo, H.B., Fornerod, M., Pieters, R., and Zwaan, C.M. (2016). Recurrent translocation t(10;17)(p15;q21) in minimally differentiated acute myeloid leukemia results in ZMYND11/MBTD1 fusion. Genes, Chromosomes and Cancer *55*, 237-241.

Döhner, H., Longo, D.L., Weisdorf, D.J., and Bloomfield, C.D. (2015). Acute Myeloid Leukemia. New England Journal of Medicine *373*, 1136-1152.

Doyon, Y., and Côté, J. (2016). Preparation and Analysis of Native Chromatin-Modifying Complexes. *573*, 303-318.

Fagnocchi, L., Cherubini, A., Hatsuda, H., Fasciani, A., Mazzoleni, S., Poli, V., Berno, V., Rossi, R.L., Reinbold, R., Endele, M.*, et al.* (2016). A Myc-driven self-reinforcing regulatory network maintains mouse embryonic stem cell identity. Nature communications *7*, 11903.

Feng, J., Liu, T., Qin, B., Zhang, Y., and Liu, X.S. (2012). Identifying ChIP-seq enrichment using MACS. Nat Protoc *7*, 1728-1740.

Gao, C., Bourke, E., Scobie, M., Famme, M.A., Koolmeister, T., Helleday, T., Eriksson, L.A., Lowndes, N.F., and Brown, J.A. (2014). Rational design and validation of a Tip60 histone acetyltransferase inhibitor. Scientific reports *4*, 5372.

Gorrini, C., Squatrito, M., Luise, C., Syed, N., Perna, D., Wark, L., Martinato, F., Sardella, D., Verrecchia, A., Bennett, S.*, et al.* (2007). Tip60 is a haplo-insufficient tumour suppressor required for an oncogene-induced DNA damage response. Nature *448*, 1063-1067.

Guo, R., Zheng, L., Park, Juw W., Lv, R., Chen, H., Jiao, F., Xu, W., Mu, S., Wen, H., Qiu, J.*, et al.* (2014). BS69/ZMYND11 Reads and Connects Histone H3.3 Lysine 36 Trimethylation-Decorated Chromatin to Regulated Pre-mRNA Processing. Molecular Cell *56*, 298-310.

Hiroaki Honda, Keiyo Takubo, Hideaki Oda, Kenjiro Kosaki, Tatsuya Tazaki, Norimasa Yamasaki, Kazuko Miyazaki, Kateri A. Moore, Zen-ichiro Honda, Toshio Suda*, et al.* (2011). Hemp, an mbt domain-containing protein, plays essential roles in hematopoietic stem cell function and skeletal formation. PNAS *108*, 2468-2473.

Hnilicova, J., and Stanek, D. (2011). Where splicing joins chromatin. Nucleus *2*, 182-188.

Jacquet, K., Fradet-Turcotte, A., Avvakumov, N., Lambert, J.-P., Roques, C., Pandita, Raj K., Paquet, E., Herst, P., Gingras, A.-C., Pandita, Tej K.*, et al.* (2016). The TIP60 Complex Regulates Bivalent Chromatin Recognition by 53BP1 through Direct H4K20me Binding and H2AK15 Acetylation. Molecular Cell *62*, 409-421.

Jason L Weirather, Mariateresa de Cesare, Yunhao Wang, Paolo Piazza, Vittorio Sebastiano, Xiu-Jie Wang, David Buck, and Au, K.F. (2017). Comprehensive comparison of Pacific Biosciences and Oxford Nanopore Technologies and their applications to transcriptome analysis. F1000Research *6:100*.

Jitka Eryilmaz, Patricia Pan, Maria F. Amaya, Abdellah Allali-Hassani, Aiping Dong, A., M., Adams-Cioaba, Farrell MacKenzie, Masoud Vedadi, and Min., J. (2009). Structural Studies of a Four-MBT Repeat Protein MBTD1. PLoS One *4*.

Langmead, B., Trapnell, C., Pop, M., and Salzberg, S.L. (2009). Ultrafast and memory-efficient alignment of short DNA sequences to the human genome. Genome Biol *10*, R25.

Li, H. (2018). Minimap2: pairwise alignment for nucleotide sequences. Bioinformatics *34*, 3094-3100.

Liao, Y., Smyth, G.K., and Shi, W. (2014). featureCounts: an efficient general purpose program for assigning sequence reads to genomic features. Bioinformatics *30*, 923-930.

TCGA Research Network (2013). Genomic and Epigenomic Landscapes of Adult De Novo Acute Myeloid Leukemia. New England Journal of Medicine *368*, 2059-2074.

Padella, A., Simonetti, G., Paciello, G., Giotopoulos, G., Baldazzi, C., Righi, S., Ghetti, M., Stengel, A., Guadagnuolo, V., De Tommaso, R.*, et al.* (2019). Novel and Rare Fusion Transcripts Involving Transcription Factors and Tumor Suppressor Genes in Acute Myeloid Leukemia. Cancers *11*, 1951.

Plesa, A., and Sujobert, P. (2019). Cannibalistic acute myeloid leukemia with ZMYND11-MBTD1 fusion. Blood *133*, 1789-1789.

Pradhan, S.K., Su, T., Yen, L., Jacquet, K., Huang, C., Cote, J., Kurdistani, S.K., and Carey, M.F. (2016). EP400 Deposits H3.3 into Promoters and Enhancers during Gene Activation. Mol Cell *61*, 27-38.

Ravens, S., Yu, C., Ye, T., Stierle, M., and Tora, L. (2015). Tip60 complex binds to active Pol II promoters and a subset of enhancers and co-regulates the c-Myc network in mouse embryonic stem cells. Epigenetics & chromatin *8*, 45.

Robinson, M.D., McCarthy, D.J., and Smyth, G.K. (2010). edgeR: a Bioconductor package for differential expression analysis of digital gene expression data. Bioinformatics *26*, 139-140.

Steunou A-L, Rossetto D, and J., C. (2014). Regulating Chromatin by Histone Acetylation. . In: Workman JL, Abmayr SM, editors Fundamentals of Chromatin Springer; New York:, pp. 147–212.

Sugden, B., Ponnusamy, R., Khatri, R., Correia, P.B., Wood, C.D., Mancini, E.J., Farrell, P.J., and West, M.J. (2019). Increased association between Epstein-Barr virus EBNA2 from type 2 strains and the transcriptional repressor BS69 restricts EBNA2 activity. PLOS Pathogens *15*, e1007458.

Tempescul, A., Guillerm, G., Douet-Guilbert, N., Morel, F., Le Bris, M.-J., and De Braekeleer, M. (2007). Translocation (10;17)(p15;q21) is a recurrent anomaly in acute myeloblastic leukemia. Cancer Genetics and Cytogenetics *172*, 74-76.

Velasco, G., Grkovic, S., and Ansieau, S. (2006). New Insights into BS69 Functions. Journal of Biological Chemistry *281*, 16546-16550.

Wang, J., Qin, S., Li, F., Li, S., Zhang, W., Peng, J., Zhang, Z., Gong, Q., Wu, J., and Shi, Y. (2014). Crystal structure of human BS69 Bromo-ZnF-PWWP reveals its role in H3K36me3 nucleosome binding. Cell Research *24*, 890-893.

Wen, H., Li, Y., Xi, Y., Jiang, S., Stratton, S., Peng, D., Tanaka, K., Ren, Y., Xia, Z., Wu, J.*, et al.* (2014). ZMYND11 links histone H3.3K36me3 to transcription elongation and tumor suppression. Nature *508*, 263-268.

Winters, A.C., and Bernt, K.M. (2017). MLL-Rearranged Leukemias-An Update on Science and Clinical Approaches. Front Pediatr *5*, 4.

Yamamoto, K., Yakushijin, K., Ichikawa, H., Kakiuchi, S., Kawamoto, S., Matsumoto, H., Nakamachi, Y., Saegusa, J., Matsuoka, H., and Minami, H. (2018). Expression of a novel ZMYND11/MBTD1 fusion transcript in CD7+CD56+acute myeloid leukemia with t(10;17)(p15;q21). Leukemia & Lymphoma *59*, 2706-2710.

Zhang, H., Devoucoux, M., Song, X., Li, L., Ayaz, G., Cheng, H., Tempel, W., Dong, C., Loppnau, P., Côté, J.*, et al.* (2020). Structural Basis for EPC1-Mediated Recruitment of MBTD1 into the NuA4/TIP60 Acetyltransferase Complex. Cell Reports *30*, 3996-4002.e3994.

Zhao, Z., Wang, L., Volk, A.G., Birch, N.W., Stoltz, K.L., Bartom, E.T., Marshall, S.A., Rendleman, E.J., Nestler, C.M., Shilati, J.*, et al.* (2019). Regulation of MLL/COMPASS stability through its proteolytic cleavage by taspase1 as a possible approach for clinical therapy of leukemia. Genes Dev *33*, 61-74.

Zjablovskaja, P., and Florian, M.C. (2019). Acute Myeloid Leukemia: Aging and Epigenetics. Cancers *12*, 103.

FIGURE LEGENDS

Figure 1: The ZMYND11-MBTD1 fusion protein is stably incorporated within the endogenous NuA4/TIP60 acetyltransferase complex.

A. Schematic representation of MBTD1, WT ZMYND11, truncated ZMYND11 and ZMYND11-MBTD1 fusion. The loss of the C-terminal MYND domain in ZMYND11 is seen in both truncated ZMYND11 and the ZMYND11-MBTD1 fusion.

B. Schematic representation of the NuA4/TIP60 complex showing where the physical link between MBTD1 and ZMYND11 is created by the fusion (made with BioRender).

C. Whole-cell extract of isogenic K562 cells stably expressing MBTD1-3xFlag 2xStrep, WT ZMYND11-3xFlag2xStrep, truncated (tr)ZMYND11-3xFlag2xStrep and the ZMYND11-MBTD1 fusion-3xFlag2xStrep from the *AAVS1* safe harbor locus. Mock is a control cell line expressing an empty 3xFlag2xStrep tag (* non-specific band).

D. Tandem affinity purifications from nuclear extracts of the cell lines shown in (C). The biotin elutions from the Strep-Tactin beads were analyzed on 4-12% SDS-PAGE followed by silver staining. Zmynd11 and subunits of the NuA4/TIP60 complex are labeled and were all identified by mass spectrometry (Table S1).

E. Purified complexes from (D) were analyzed by western blot with the indicated antibodies to confirm the presence of known subunits of the NuA4/TIP60 complex.

See also Table S1.

Figure 2: The ZMYND11-MBTD1 fusion binds ZMYND11-targets in the genome, enriched on gene bodies, affecting chromatin acetylation and RNA pol II signals on specific genes.

A. Average of enrichment of MBTD1, WT ZMYND11, truncated (tr.) ZMYND11 and ZMYND11-MBTD1 fusion plotted to the genomic regions as promoters, exon, intron, intergenic and other (5’UTR and 3’UTR). Genome-wide localization of the fusion was

analyzed by ChIP-seq and compared to data obtained in parallel with MBTD1, WT ZMYND11 and truncated (tr.) ZMYND11. Anti-Flag chromatin immunoprecipitations were performed in tagged and mock K562 cell lines used in figure 1.

B. Comparison of genomic binding loci of truncated (tr.) ZMYND11, WT ZMYND11, MBTD1, and ZMYND11-MBTD1 fusion highlights extensive common targets between ZMYND11 and the fusion protein. Furthermore, truncated ZMYND11 can still bind the full set of ZMYND11 targets despite the loss of the MYND domain.

C. Examples of ZMYND11-MBTD1 binding profiles on ZMYND11-target genes *RPSA*, *MYC* oncogene, *FASTK* and *TMUB1*, compared to WT and truncated ZMYND11, as well as MBTD1 and mock control. Note MBTD1 binding to the *RPSA* promoter.

D. ChIP-qPCR confirms the localization of ZMYND11-MBTD1 on ZMYND11 target-genes (coding regions). *RPSA* prmoter is used as control for the NuA4/TIP60 complex (MBTD1). Error bars represent range of two independent experiments.

E. ChIP-qPCR of acetylated histone H4 in the different K562 cell lines. Signals are presented as a ratio of IP/input % of H4ac on total H3 to correct for nucleosome occupancy. The expression of ZMYND11-MBTD1 fusion increases the acetylation of H4 on the coding region of specific bound-genes, as *MYC* and *TMUB1*. Error bars represent the range based on two independent experiments.

F. ChIP-qPCR of H4 acetylation along the body of the *MYC* gene, showing an increase of acetylation over the central exon specific to the cells expressing ZMYND11-MBTD1, precisely where the fusion protein is localized. The set of primers used are shown in the schematic *MYC* locus. Error bars represent the range of two independent experiments.

G.H. ChIP-qPCR of RNA polymerase II (RNAPII) signals are presented as a ratio of IP/input % on a negative control locus (*MYOD*). The set of primers used are shown in the schematic

RPSA locus (G) or *MYC* locus (H), respectively. Error bars represent the range of two independent experiments.

Statistical analyses were performed by two-way ANOVA test followed by Tukey's test, *, $p < 0.05$, **, $p < 0.01$, ***, $p < 0.001$, ****, $p < 0.0001$

See also Fig. S1

Figure 3: Expression of the ZMYND11-MBTD1 fusion leads to changes in expression of several hundred genes, including *MYC* and *AKT2*, as well as transcript isoforms produced by alternative splicing.

A. 340 genes are found upregulated (left) and 446 downregulated (right) by expression of ZMYND11-MBTD1 after comparison with truncated ZMYND11 and MBTD1 in KO ZMYND11 cell lines and control cell line with WT ZMYND11 (p-value 0.01% and 25% FDR). mRNA from 2 clones of each cell line were analyzed for differential expression by long range RNA-seq.

B. Gene ontology (GO) analysis for upregulated and downregulated genes using string-db software (FDR < 0.005).

C. RT-qPCR of *MYC* and *AKT2* expression in the different cell lines, confirming the ZMYND11-MBTD1-driven upregulation detected by RNA-seq. Error bars represent the range of two biological replicates.

D. Scatter plots comparing gene and transcript expressions (log2 fold changes (FC)) in cells expressing ZMYND11-MBTD1 fusion versus its control partners (MBTD1 and truncated ZMYND11 (trunc)) in the endogenous ZMYND11 KO background. Dots represented transcripts and genes that are significantly changed (blue dots) or not (grey dots). Orange dots represented 150 common transcripts differentially expressed with the fusion compared to both controls, MBTD1 and tr. ZMYND11.

E-F. Canonical and spliced isoforms of *NAT14* and *SCAMP4* mRNAs measured by RT-qPCR and normalised to *RPLP0*. NAT14-204 transcript and SCAMP4-204 transcript are upregulated and downregulated, respectively, in cells expressing the fusion compared to control cell lines. Values represent means relative to control cell lines from two biological replicates and error bars are range.

Statistical analyses were performed by two-way ANOVA test followed by Tukey's test, *, $p < 0.05$, **, $p < 0.01$, ***, $p < 0.001$.

See also Fig. S2

Figure 4. The ZMYND11-MBTD1 fusion protein favors Myc-dependent pluripotency and inhibits expression of differentiation markers.

A. MBTD1 and ZMYND11 loose their growth inhibition activity measured by clonogenic assay when physically linked in the ZMYND11-MBTD1. Clonogenic assay was performed in U2OS cells transfected with the indicated expression vectors or empty vector, for 48h (expression verified in Fig. S2D). Error bars represent the range of two independent experiments. Statistical analyses were performed by two-way ANOVA test followed by Tukey's test, **, $p < 0.01$, ***, $p < 0.001$.

B. Relative transcriptional levels of the indicated genes after expression of the fusion in mouse embryonic stem cells (mESCs). Empty vector, MBTD1, WT ZMYND11 and truncated (tr.) ZMYND11 are used as control. *Pax3* is a marker for differentiation while *Stella*/*Dppa3* and *MYC* are pluripotency markers (see expression of the constructs and full set of genes tested in Fig. S2E-G).

C. Model for the oncogenic mechanism of the ZMYND11-MBTD1 fusion. Expression of the ZMYND11-MBTD1 leds to its stable association with the endogenous NuA4/TIP60 complex, thereby mistargeting this complex to the coding region of specific genes such

as the *MYC* oncogene which is upregulated. This mistargeting leads to changes not only in chromatin dynamics on specific genes but also in mRNA processing, likely due in part to the absence of ZMYND11 MYND domain in the fusion (made with BioRender).

Devoucoux Figure 1

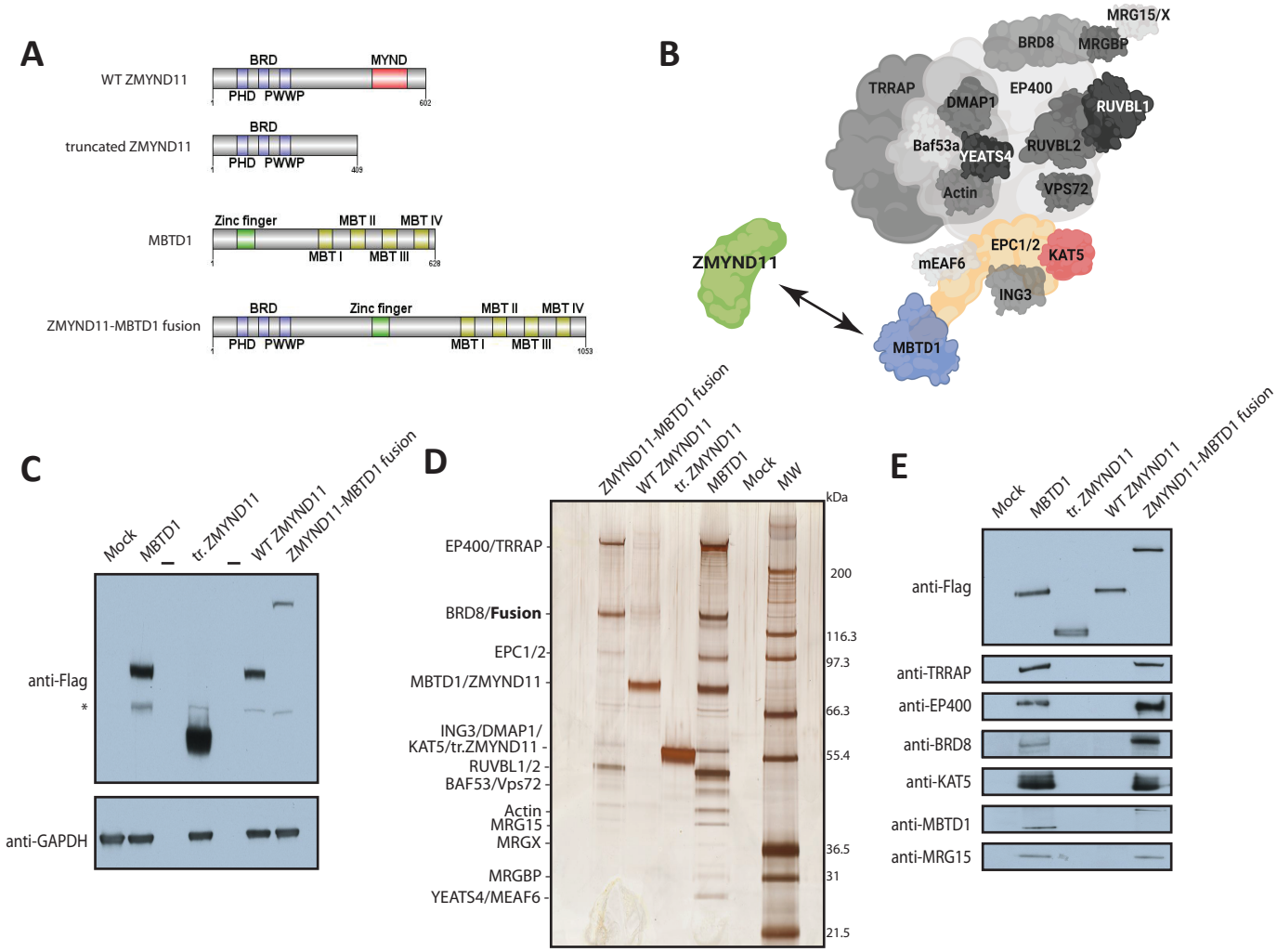

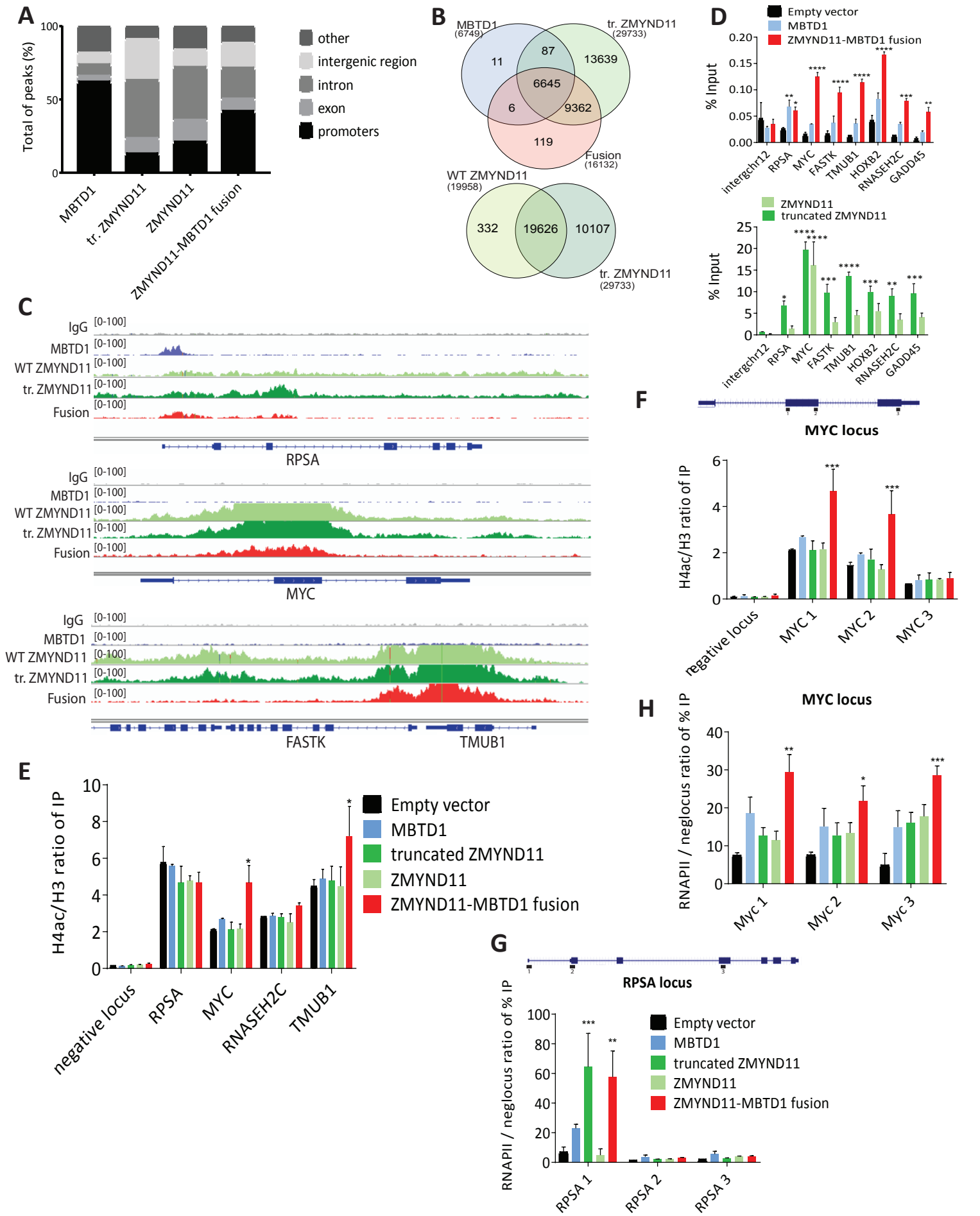
A
Total of peaks (%)
100
50
0
MBTD1
tr. ZMYND11
ZMYND11
ZMYND11-MBTD1 fusion
other
intergenic region
intron
exon
promoters
B
MBTD1 (6749)
tr. ZMYND11 (29733)
Fusion (16132)
11
87
13639
6645
6
9362
119
WT ZMYND11 (19958)
tr. ZMYND11 (29733)
332
19626
10107
C
IgG
MBTD1
WT ZMYND11
tr. ZMYND11
Fusion
[0-100]
RPSA
MYC
FASTK
TMUB1
D
Empty vector
MBTD1
ZMYND11-MBTD1 fusion
% Input
intergchr12
RPSA
MYC
FASTK
TMUB1
HOXB2
RNASEH2C
GADD45
ZMYND11
truncated ZMYND11
E
H4ac/H3 ratio of IP
negative locus
RPSA
MYC
RNASEH2C
TMUB1
Empty vector
MBTD1
truncated ZMYND11
ZMYND11
ZMYND11-MBTD1 fusion
F
MYC locus
H4ac/H3 ratio of IP
negative locus
MYC 1
MYC 2
MYC 3
G
RPSA locus
RNAPII / neglocus ratio of % IP
RPSA 1
RPSA 2
RPSA 3
Empty vector
MBTD1
truncated ZMYND11
ZMYND11
ZMYND11-MBTD1 fusion
H
MYC locus
RNAPII / neglocus ratio of % IP
Myc 1
Myc 2
Myc 3

Devoucoux Figure 3

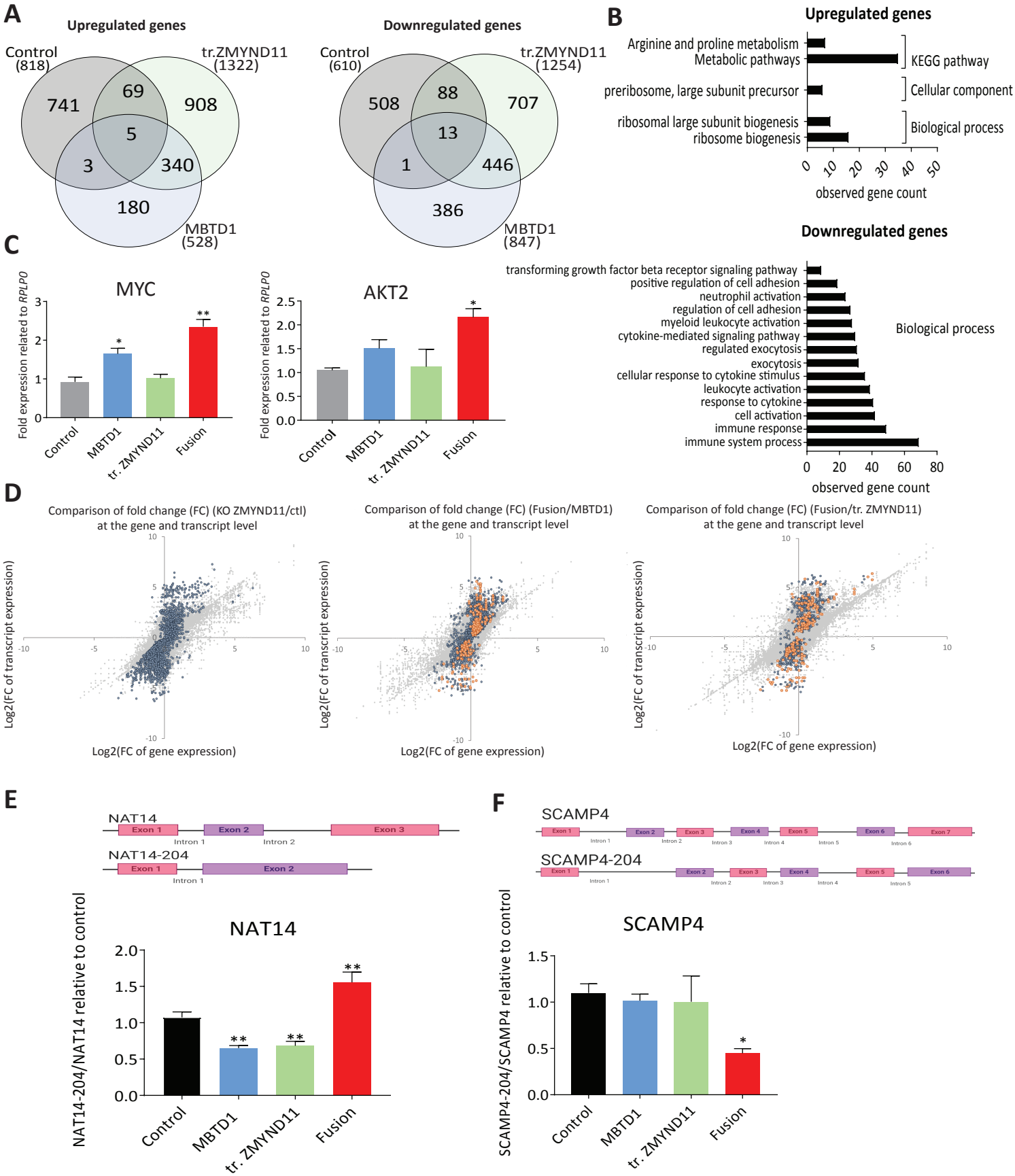

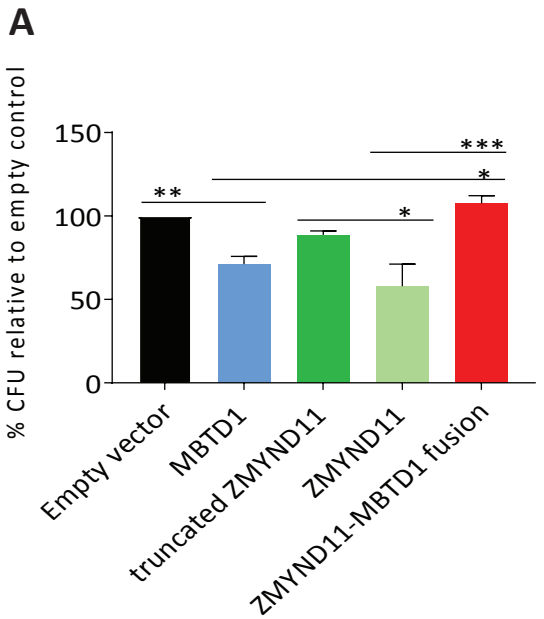
A
% CFU relative to empty control
150
100
50
0
**
*
*
***
Empty vector
MBTD1
truncated ZMYND11
ZMYND11
ZMYND11-MBTD1 fusion

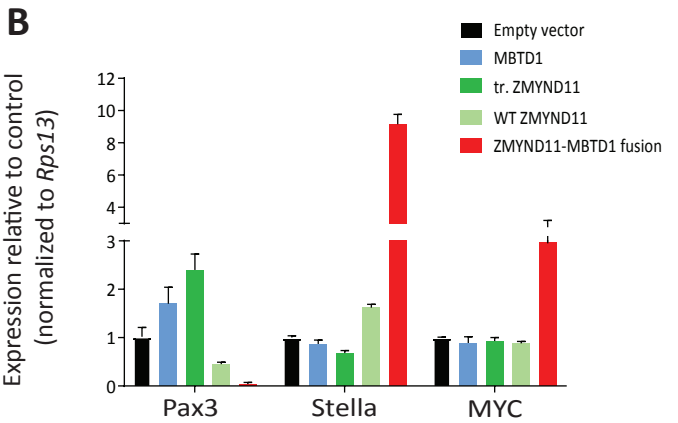
B
Expression relative to control
(normalized to Rps13)
12
10
8
6
4
3
2
1
0
Empty vector
MBTD1
tr. ZMYND11
WT ZMYND11
ZMYND11-MBTD1 fusion
Pax3
Stella
MYC

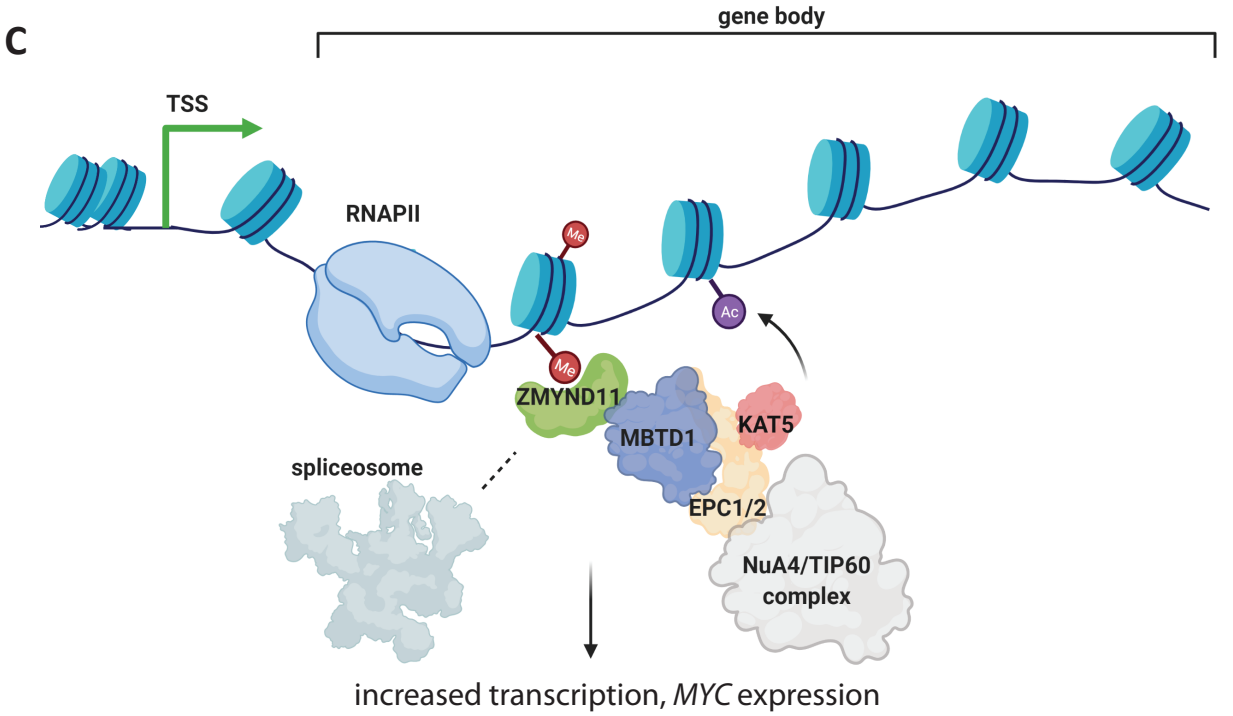
C
gene body
TSS
RNAPII
Me
Me
Ac
ZMYND11
MBTD1
KAT5
EPC1/2
NuA4/TIP60
complex
spliceosome
increased transcription, MYC expression

SUPPLEMENTARY FIGURE LEGENDS

Figure S1. The ZMYND11-MBTD1 fusion protein associates with the gene bodies.

Related to figure 2.

A. Average ChIP-seq profiles of binding peaks in the vicinity of acceptor and donor splice sites. Genes are separated by gene expression quantiles (Q4 is the highest expression). MBTD1 is not enriched in this genomic region compared to the three others, WT ZMYND11, truncated (tr.) ZMYND11, and the fusion.
B. Gene Ontology (GO) term enrichment analysis using DAVID 6.8 shows terms for biological processes, molecular function and KEGG pathway (FDR ≤ 0.01) enriched in ZMYND11-MBTD1 fusion and truncated ZMYND11 but not MBTD1.
C. Representative ChIP tracks of the ZMYND11-MBTD1 fusion showing its localization on the coding region of *HOXB2*, *RNASEH2C* and *GADD45A*, respectively. Genome-wide ZMYND11-MBTD1 fusion localization was analyzed after ChIP-seq and compared to data obtained in parallel with IgG control, MBTD1, WT ZMYND11, and truncated (tr.) ZMYND11.
D. ChIP-qPCR of H3K4me3 from K562 cells stably expressing MBTD1, WT ZMYND11, truncated ZMYND11 and ZMYND11-MBTD1 fusion. Signals are presented as a ratio of %IP/input on total H3 to correct for nucleosome occupancy, at the *MYC* gene and *MYOD* as negative control. Error bars represent the range on two independent experiments.
E. ChIP-qPCR of H3K36me3 from cells in C at different locations along the *MYC* and *RPSA* genes. *MYOD* is used as negative control. Signals are presented as a ratio of %IP/input on total H3 to correct for nucleosome occupancy and error bars represent the range based on two independent experiments. Statistical analyses were performed by two-way ANOVA test followed by Tukey's test, **, $p < 0.01$.

Figure S2: Construction of ZMYND11 KO cell lines for transcriptomics and effect of ZMYND11-MBTD1 expression on cell fate.

Related to figures 3 and 4.

A. ZMYND11 DNA sequence showing both gRNAs used to generate a truncation in the MYND domain of ZMYND11 (in purple and in blue).

B. Selection of ZMYND11 knock-out (KO) clones. Results of a PCR-based screening on genomic DNA to detect CRISPR-mediated deletion in single-cell-derived K562 clones after ouabain selection. Two homozygote KO clones are shown for each AAVS1 cell line (MBTD1, truncated (tr.) ZMYND11 and ZMYND11-MBTD1 fusion (fusion)). Alleles were also sequenced to verify the accurate deletion in each KO clone.

C. RT-qPCR to measure ZMYND11 expression in the different KO clones isolated. 2 sets of primers were used in N-term and C-term of the *ZMYND11* coding sequence. Signals are presented as a fold expression relative to *RPLP0* control.

D. Overexpression of ZMYND11-MBTD1 fusion for clonogenic assays in U2OS cells. MBTD1, truncated (tr.), and WT ZMYND11 are used as control. U2OS cells were transfected in duplicates with those constructs or empty vector for 48h following puromycin selection.

E. Overexpression of ZMYND11-MBTD1 fusion in mouse embryonic stem cells (mESCs). MBTD1, truncated ZMYND11 (tr. ZMYND11), WT ZMYND11 and empty vector are used as control. mESCs were transfected in duplicates, selected for 48h with puromycin before spontaneous differentiation.

F. RT-qPCR of indicated pluripotency markers after overexpression of the ZMYND11-MBTD1 fusion in mESCs. MBTD1, WT ZMYND11, truncated (tr.) ZMYND11 and empty vector were used as control.

G. RT-qPCR of indicated differentiation markers for specific germ layers in mESCs after overexpression of empty vector, MBTD1, WT ZMYND11, truncated (tr.) ZMYND11 and ZMYND11-MBTD1 fusion. Note the fusion-specific drop in Brachyury expression compared to controls.

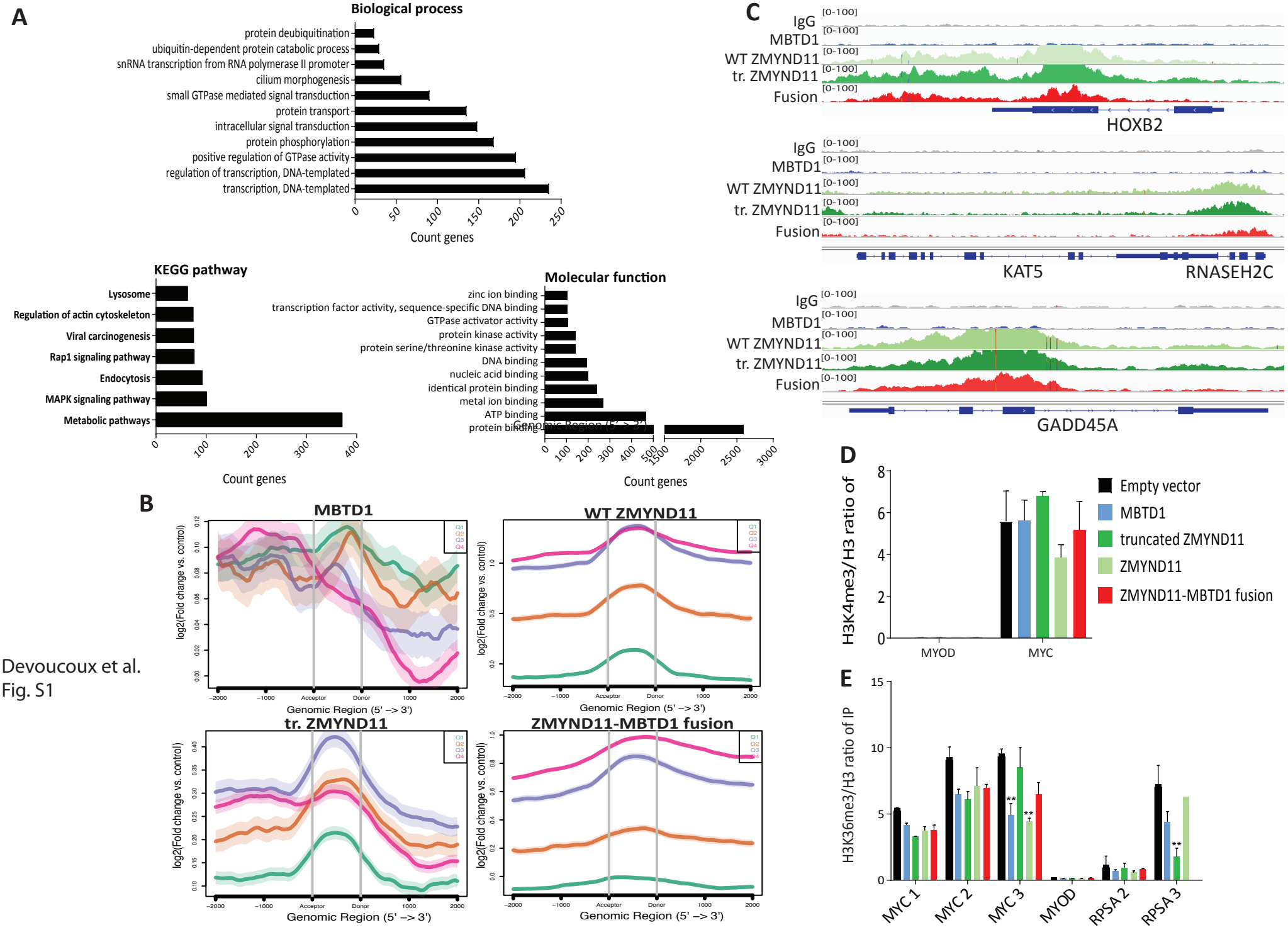

Devoucoux et al.
Fig. S1

A

> ZMYND11 seq.- 1003 bp

attatgtggcttcgtttggcgtctaaactcttgtctcacctttttagGAACCAGAGCCT-
GAAACAGAAGCAGTAAGTTCTAGCCAGGAAATACCCACGATGCCTCAGCCCATCGAA
AAAGTCTCCGTGTCAACTCAGACAAAGAAGTTAAGTGCCTCTTCACCAAGAATGCTG
CATCGGAGCACCCAGACCACAAACGACGGCGTGTGTCAGAGCATGTGCCATGACAAA
TACACCAAGATCTTCAATGACTTCAAAGACCGGATGAAGTCGGACCACAAGCGGGAG
ACAGAGCGTGTTGTCCGAGAAGCTCTGGAGAAGgtaatgcttgtcgccactgtgggtgccctg
ctgcagccggcactcctgtcatggttaggctcctttcactcatgcatcaacccagtagcagcttttacatgtagc
catataatgacaccagtatcttttacagcatttcaagtaataatgatactttcctcacctaaatttttacacatgta
atgaaggggaaaaaaggtacctcatgcaagttgtgttaagtttctgttccagtgtagatggtctgtgttaagtt
gtgtgctgacgcactgtgggttgtcttttcattccagCTGCGTTCTGAAATGGAAGAAGAAAAGA
GACAAGCTGTAAATAAAGCTGTAGCCAACATGCAGGGTGAGATGGACAGAAAATGTA
AGCAAGTAAAGGAAAAGTGTAAGGAAGAATTTGTAGAAGAAATCAAGAAGCTGGCA
ACACAGCACAAGCAACTGATTTCTCAGACCAAGAAGAAGCAGTGGgtaaataccagtctt
ttttagacccttatttctgaaaatgtaccacaggtatgatgcccgttaattcagaaggtagctgtggcacatgca
gaagatgtttctgaaataagatcaaatgtgaaatggtcagctttagttttaaaaatttattaaaagtcctatgat
ctctcaaccccagatcccatattactgtgtactgctca

B

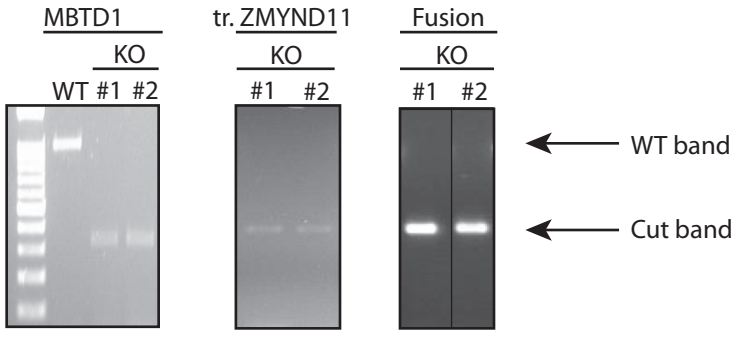

C

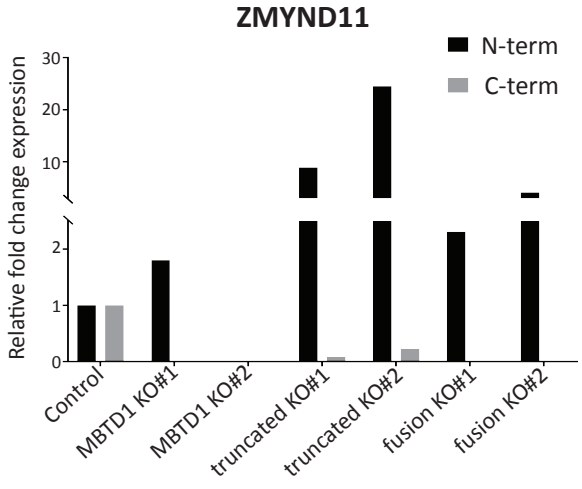

D

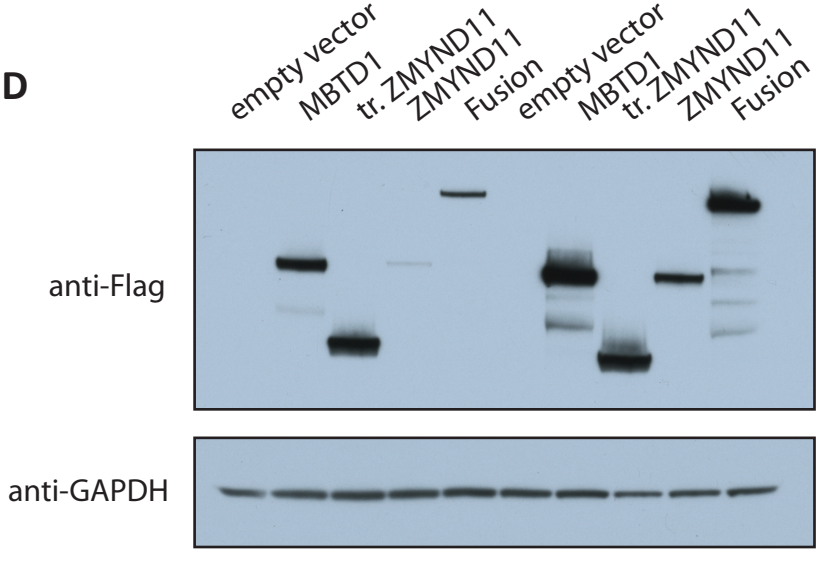

E

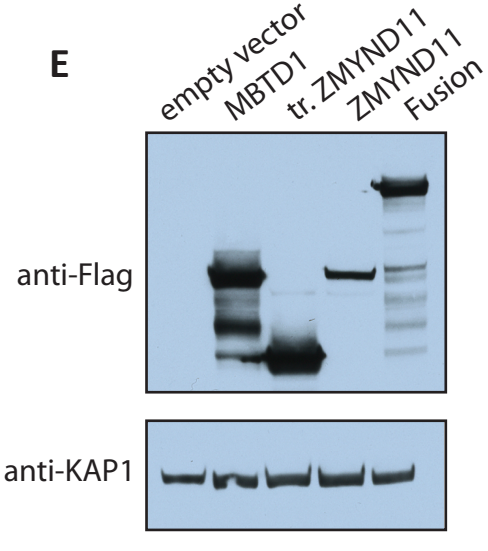

Devoucoux et al.
Fig. S2

F

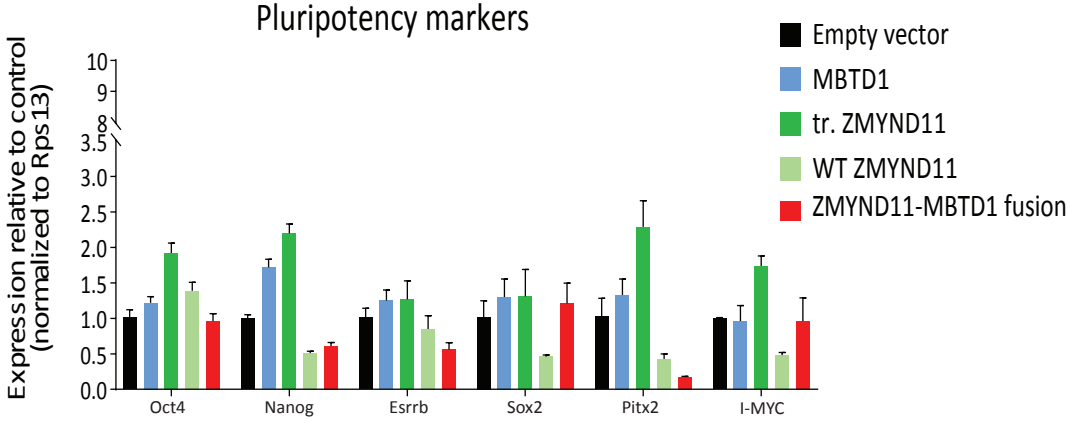

G

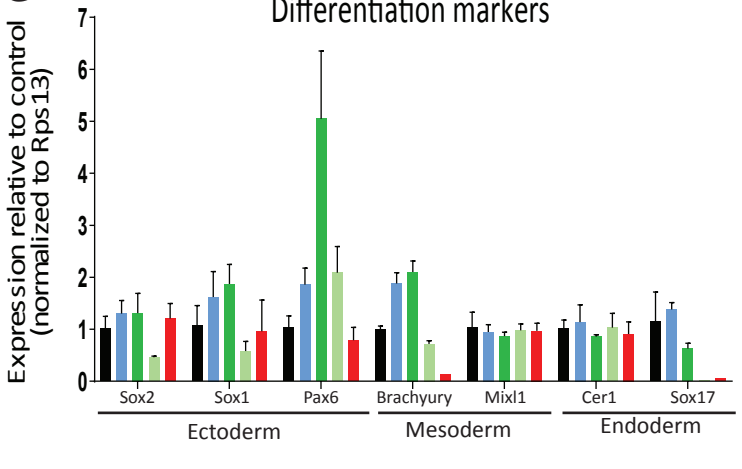

Supplemental Table S1: Mass spectrometry analysis of TIP60 complex (left) and ZMYND11 interactome (right) purified from K562 cells through MBTD1- full lenght (WT) or truncated (tr.) ZMYND11- and the ZMYND11-MBTD1 fusion-3xFlag2xStrep integrated at AAVS1 (total spectral count). ZMYND11 interactors previously identified by *Guo et al, Mol Cell, 2014* are indicated in bold. Related to Fig. 1

	Protein name	MW	MBTD1	WT ZMYND11	Fusion
NuA4/TIP60 complex	TRRAP	438 kDa	541	0	233
	EP400	336 kDa	449	0	216
	BRD8	97 kDa	78	0	32
	EPC1	93 kDa	89	0	42
	EPC2	91 kDa	82	0	37
	MBTD1	71 kDa	107	0	75
	KAT5	59 kDa	36	0	16
	DMAP1	53 kDa	68	0	42
	RUVBL2	51 kDa	145	0	76
	RUVBL1	50 kDa	108	0	56
	ACT6LA	47 kDa	53	0	30
	ING3	45 kDa	47	0	17
	ACTB	42 kDa	67	0	45
	VPS72	41 kDa	22	0	11
	MORF4L1	37 kDa	25	0	11
	MORF4L2	32 kDa	23	0	12
	YEATS4	27 kDa	30	0	20
	MRGBP	22 kDa	14	0	10
	MEAF6	22 kDa	9	0	4
	ZMYND11	71 kDa	0	161	36

			ZMYND11 (1)		ZMYND11 (2)	
	Protein name	MW	truncated	WT	truncated	WT
	ZMYND11	71 kDa	90	161	431	220
mRNA processing	**SRRM2**	300 kDa	0	46	3	26
	ACIN1	147 kDa	0	18	0	17
	NAT10	116 kDa	0	7	0	4
	EFTUD2	109 kDa	0	7	3	7
	NOP14	98 kDa	0	6	1	2
	TFIP11	97 kDa	0	2	0	2
	ZC3H18	84 kDa	0	7	0	10
	PNN	82 kDa	0	11	2	7
	PPIG	40 kDa	0	6	0	2
chromatin-remodeling	KMT2A	432 kDa	0	7	0	3
	KDM3B	192 kDa	0	18	0	10
	L3MBTL2	79 kDa	0	20	2	16
	PBRM1	193 kDa	0	2	0	5
	SMARCA4	189 kDa	0	3	1	5
	SMARCA5	122 kDa	0	3	0	4
	TOP2B	183 kDa	0	11	0	4
	TOP2A	174 kDa	0	20	2	11
	PELP1	125 kDa	0	4	0	7
	AKAP8	76 kDa	0	5	0	9
	H3	14 kDa	0	4	2	6
	H2B	14 kDa	0	2	2	2
	H4	11 kDa	0	4	1	3

Supplemental Table S2: A. ChIP-sequencing analysis and C. Long reads MinION/Expression analysis of the ZMYND11-MBTD1 fusion in K562: histone marks and transcription factors enriched on genes that bound by ZMYND11-MBTD1 fusion protein and truncated ZMYND11 but not MBTD1 (ENCODE Histone modifications 2015; EnrichR and ENCODE Transcription Factors ChIP-seq 2015; EnrichR, respectively). B. Correlation between ChIP-seq and long read RNA-seq data. Among 340 upregulated genes, 197 are found targeted by the ZMYND11-MBTD1 fusion and among 446 downregulated genes, 204 are found targeted by the the fusion. Related to figure 2 and figure 3.

A

Term	Overlap	P-value	Combined Score
H3K79me2	606/2000	0.002389249	6.996375132
H3K9ac	1000/3409	0.006484132	5.592278804
H3K27ac	581/2000	0.064235538	2.975704311
TBP	613/2000	7.25E-04	8.533975762
TAF1	474/1543	0.002417396	7.108044886
POLR2AphosphoS5	445/1459	0.005517928	6.061480947
FOS	600/2000	0.00603442	5.829028642
NFYA	597/2000	0.009281678	5.295414888

B

	Number of genes	Total of genes
upregulated	197	340
downregulated	204	446

C

Term	Overlap	P-value	Combined score
H3K36me3	63/2634	0.004208435902329572	7.5853519935991525
MAX	89/3845	0.0015475727414263065	8.683213838232108
MYC	141/6800	0.004283665457326099	6.554692387981143